Published in the Proceedings of the 16th International Aluminum Alloys Conference (ICAA16) 2018
ISBN: 978-1-926872-41-4
by the Canadian Institute of Mining, Metallurgy & Petroleum

FOUR REGIONS IN LOW-TEMPERATURE CREEP OF ULTRAFINE-GRAINED ALUMINUM

*Eiichi Sato[1], Kenta Higane[1], Hiroshi Masuda[1], and Koichi Kitazono[2]

[1] *Institute of Space and Astronautical Science, JAXA*
Yoshinodai, Sagamihara, Japan
*(*Corresponding author: sato@isas.jaxa.jp)*

[2] *Graduate School of System Design, Tokyo Metropolitan University*
Hino, Tokyo, Japan

ABSTRACT

The present study investigated the low-temperature creep mechanisms in ultrafine-grained (UFG) aluminum manufactured by accumulative roll bonding. UFG aluminum with grain size 0.39 μm showed steady state creep even at room temperature under low stresses as confirmed by the creep curves in the strain rate–strain plot. The low-temperature behavior was divided into four regions by three distinctive stresses, σ_I, σ_{II} and σ_{III}: σ_I (=45 MPa) is denoted as the micro-yielding stress with which dislocations start movement, σ_{II} (=85 MPa) the dislocation-multiplication stress above which dislocations multiply with creep deformation, and σ_{III} (=171 MPa) the conventional yield stress above which macroscopic plastic strain is generated. During low-temperature creep, below σ_I, negligible plastic strain is generated. Between σ_I and σ_{II}, creep deformation with stress exponent 2.5 occurred, which is accommodated by dislocation absorption into grain boundary and grain boundary sliding, similarly to the low-temperature creep of HCP metals. Between σ_{II} and σ_{III}, creep deformation with stress exponent 7.0 occurred, whose mechanism is similar to the low-temperature creep of coarse-grained aluminum. Above σ_{III}, power-law breakdown occurred.

KEYWORDS

Aluminum, Ultrafine grained (UFG), Low-temperature creep, Micro-yielding, Dislocation

INTRODUCTION

It is well understood that the creep deformation brings about at high homologous temperatures (T/T_m) of >0.4, where T_m is the melting point, with diffusion processes. Recently, the importance of aluminum is increasing for cryogenic temperature parts such as a metallic liner or a cap in high pressure-hydrogen vessels, and the presence of creep behavior in aluminum at room temperature has become recognized (Matsunaga, 2013; Kassner, 2015).

In HCP metals and alloys, especially in titanium, steady-state creep behavior appears at room temperature with apparent activation energy of 1/10 of that for self-diffusion (Neeraj, 2000; Matsunaga, 2009). On the other hand, Kassner (2015) claims that aluminum shows creep behavior at room temperature with apparent activation energy of 4/5 of that for self-diffusion, but never reaches the steady state. We should note that it is derived from the data obtained from short-term creep tests of few hour, and Matsunaga (2013) already claimed the presence of steady state in room temperature creep in aluminum with activation energy of 1/5 of that for self-diffusion.

The mechanisms for low temperature creep are considered different between HCP and FCC metals: in HCP metals, grain boundary sliding is observed and is thought to accommodate piled-up dislocations at grain boundaries through absorbing them. The so-called slip-induced grain boundary sliding occurs with low number of activated slip systems (Matsunaga, 2009). On the other hand, in FCC metals, many activated slip systems bring about work hardening with dislocation cell structure formation. In the initial stage of creep, it results in primary creep (Kassner, 2015), but Matsunaga (2013) claimed that once the annihilating of a cross-slipped dislocation to another reaches balance, steady state is established. It has been, however, strongly required to show more convincing experimental verification for the presence of steady state in FCC metals at low temperature.

On the other hand, ultra-fine grained (UFG) and fine grained (FC) FCC metals do not create dislocation cell structure unlike the above mentioned coarse-grained (CG) ones (Blum, 2009). It infers a different creep behavior and mechanism working in UFG and FG FCC metals from CG ones. Low temperature creep of UFG aluminum was examined by Matsunaga (2012), inferring dislocation creep accommodated by non-diffusional process similar to HCP metals. However, that study needs creep experiment for much longer period till reaching steady state, and also lacks detailed microstructural observation. In addition, low stress level experiments are inevitable to reveal the entire understanding. This paper aims to review and summarize the entire view of low temperature creep of UFG aluminum, based on the recent study, which executed long-term creep experiments under various stress levels by the present authors (Higane, 2017).

EXPERIMENTAL

Rolled Al sheets of 1050 Al were accumulative-roll-bonded for six cycles corresponding to the equivalent strain of 4.8 without lubricants, following to the procedure by Saito (1998), and then were annealed in several conditions to get the specimens with average grain sizes of d=0.39–18 μm estimated as intercept lengths along the normal direction of the rolled sheets. All the specimens had completely recrystallized microstructures.

Tensile tests were performed for various grain-size aluminum using an Instron-type machine with a constant crosshead speed corresponding to an initial strain rate of 1.0×10^{-3} s^{-1} at 300 K to evaluate 0.2% proof stress $\sigma_{0.2}$ and micro-yielding stress σ_{my}. Creep tests were, then, conducted for various grain-size aluminum using dead-load creep frames. In the both tests, strain was measured by strain gauges attached on the specimen surface; the gages with double-tern tabs were adopted to get stable strain-rate measurement less than 10^{-11} s^{-1} through reducing long-term viscous relaxation in adhesion layer (Sato, 2005). Detailed analysis on creep behavior was performed for UFG aluminum with grain size of d=0.39 μm.

Microstructural observations were performed after creep interrupt tests of UFG aluminum of d=0.39 μm using a scanning electron microscope with electron channeling contrast image technique (SEM/ECCI) to observe dislocation structures inside of a grain and near grain boundary. The observed samples were polished mechanically and then electro-polished using 25% nitric acid and 75% methanol at 253 K and 12-15 V on the normal plane of the rolled sheet.

RESULTS

Tensile Properties

Figure 1 shows the stress σ–strain rate ε curves of various grain-size aluminum elongated with strain rate of 1.0×10^{-3} s^{-1}. Here plotted the strain estimated by crosshead displacement. It is noted that UFG aluminum of d<1 μm shows yielding phenomena, while FG and CG aluminum of 1<d<5 μm and 5 μm≤d, respectively, show no such phenomena. In addition, UFG aluminum yields certain amount of plastic strain before reaching its yield point, and that of d<0.5 μm reveals rapid fracture after yielding without revealing work hardening. These phenomena are consistent with previous studies on UFG aluminum (for example, Kawashima, 2009).

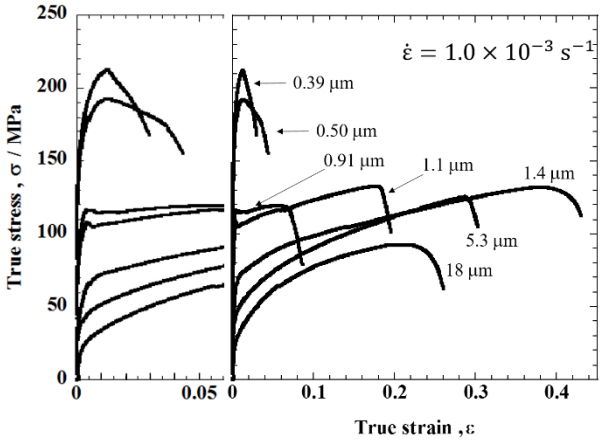

Figure 1. Stress-strain curves of various grain-size aluminum at 1.0×10^{-3} s^{-1}

Micro-yielding stresses σ_{my}, which express the stress at which dislocations start moving, were evaluated for various grain-size aluminum. That stress was obtained as the stress where apparent Young's modulus dσ/dε starts decreasing from that of aluminum, 68 MPa, as shown in Figure 2(a) as an example of typical dσ/dε versus ε curve of UFG aluminum of d=0.39 μm at strain rate of 6.4×10^{-6} s^{-1}. The obtained σ_{my} had low values of about 5 MPa in the CG region. The magnitude of σ_{my} increased in proportion to d^{-2} in the FG and UFG regions similarly to the Hall-Petch relation of yield stress.

Figure 2(b) shows the dependence of σ_{my} on strain rate in UFG aluminum of d=0.39 μm. Apparently, it decreases as strain rate decreases, though it seems to converge into 45 MPa in the low strain rate extreme. The micro-yielding stress acting in the creep condition with low strain rate as will be shown in Figure 4 is, then, considered as 45 MPa.

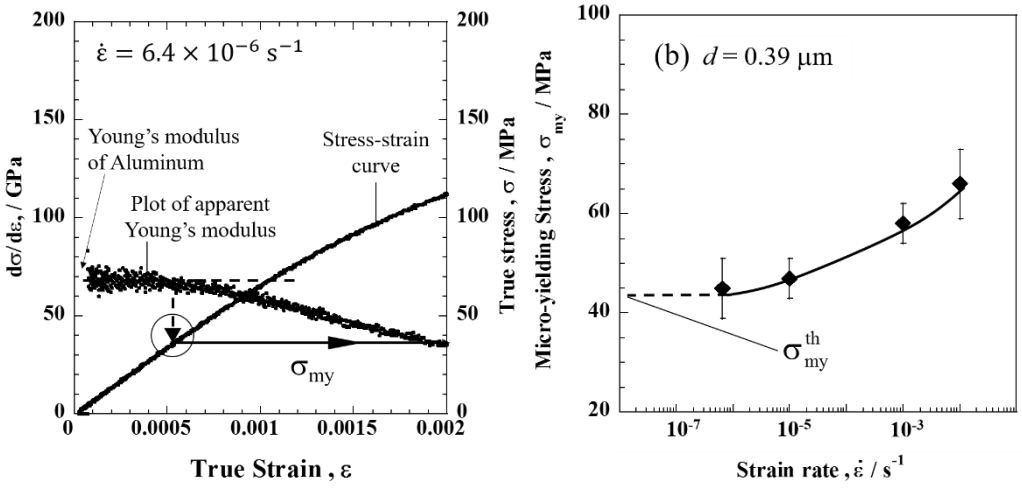

Figure 2. (a) Typical dσ/dε curve of UFG aluminum of d=0.39 μm at 6.4×10^{-6} s^{-1}
(b) Strain rate dependence of σ_{my} in UFG aluminum of d=0.39 μm

Creep Properties

Figure 3 shows the creep curves (strain ε–time t plot) of aluminum of d=0.39 μm under various stresses at room temperature. UFG aluminums shows clear creep behavior. To follow the evolution of deformation resistance in creep experiments, in Figure 4, strain rate $\dot{\varepsilon}$ is plotted in logarithm against strain ε (Blum, 1993). It is apparent that many of creep curves with stresses above 53 MPa show minimum creep rate and the following third stage creep; the steady-state creep rate was then estimated. On the other hand, with stresses below 43 MPa creep curves do not reach the steady state. Figure 5 is a double logarithmic plot of strain rate $\dot{\varepsilon}$ and modulus-compensated applied stress σ/E, where closed symbols represent the minimum creep rates and open symbols the lowest creep rates measured.

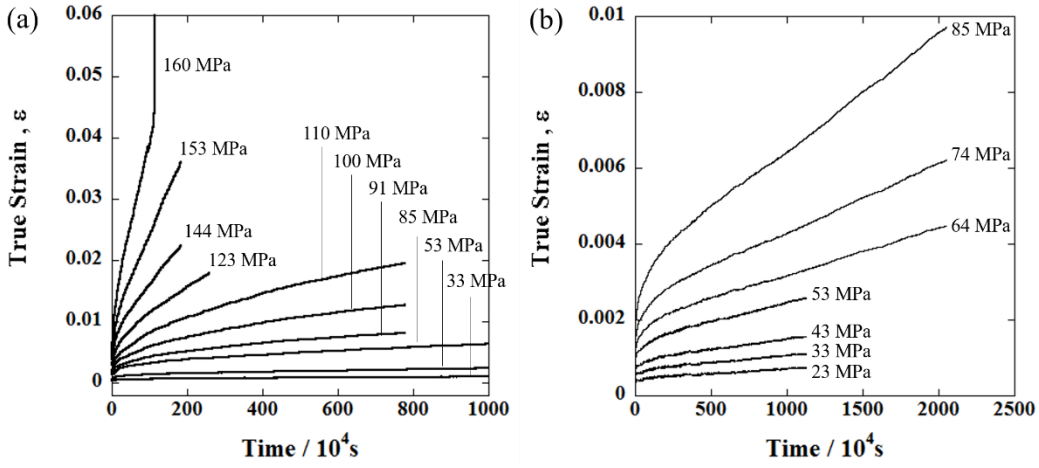

Figure 3. Creep curves of UFG aluminum of d=0.39 μm

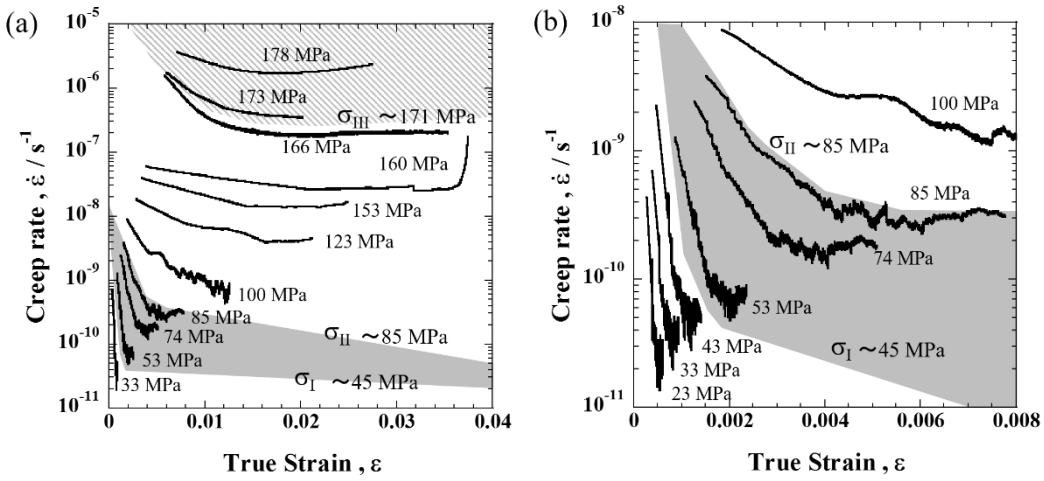

Figure 4. Creep curves in strain rate–strain plot of UFG aluminum of d=0.39 μm

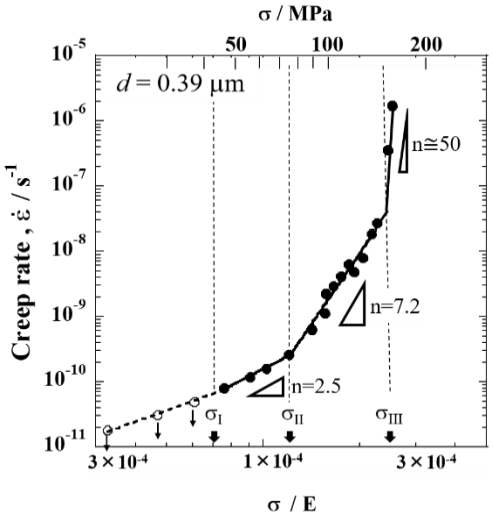

Figure 5. Dependence of steady-state creep rate on stress in UFG aluminum of d=0.39 μm

Based on the shape of creep curve in $\dot{\varepsilon}$–ε plot in Figure 4 and the value of stress exponent n=dlnε̇/dlnσ in Figure 5, low-temperature creep of UFG aluminum is devided into four regions: The boundary stresses are denoted as σ_I, σ_{II} and σ_{III} from the lower. In the lowest stress region of $\sigma<\sigma_I$, creep rate continuously decreases during creep not to reach steady state. The boundary stress σ_I is evaluated as about 45 MPa, which equals to the micro-yielding stress σ_{my} at low strain rate limit given by Figure 2(b). With higher stress than σ_I, steady state creep appears as confirmed in Figure 4, but has three different values of n. The second lowest region of $\sigma_I<\sigma<\sigma_{II}$ has n value of 2.5, while the third lowest stress region of $\sigma_{II}<\sigma<\sigma_{III}$ has that of 7.2. The boundary stess σ_{II} is determined as 85 MPa. The highest stress region corresponds to the power-law breakdown. The boundary stress σ_{III} is evaluated as 171 MPa, which corresponds to $\sigma_{0.2}$=171 MPa rather than σ_y,=212 MPa in tensile deformation shown in Figure 1.

The instantaneous plastic strain in creep $\Delta\varepsilon_0$ is plotted as a function of stress in Figure 6 for UFG aluminum of d=0.39 μm. In the lowest stress region of $\sigma<\sigma_I$, $\Delta\varepsilon_0$ is almost negligible. It increases slowly as stress increases in the second lowest stress region of $\sigma_I<\sigma<\sigma_{II}$, and then increases rapidly in the third lowest stress region of $\sigma_{II}<\sigma<\sigma_{III}$.

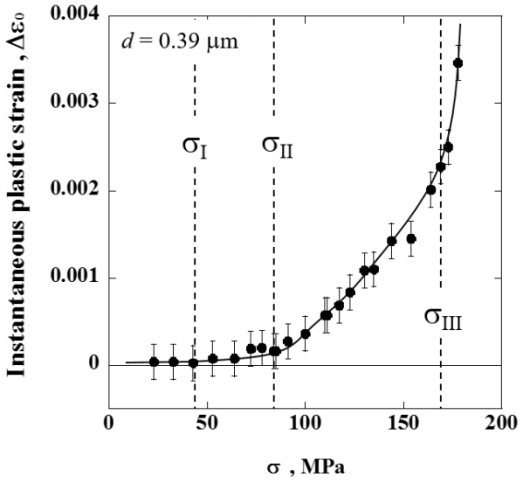

Figure 6. Instantaneous plastic strain in an UFG aluminum of d=0.39 μm under different stress levels

Microstructural Observation

Figure 7 shows SEM/ECCI images, which are taken after the creep interrupted tests at following conditions; (a) σ=53 MPa corresponding to the region of $\sigma_I<\sigma<\sigma_{II}$, interrupted at strain of ε=0.0025, and (b) σ=130 MPa corresponding to the region of $\sigma_{II}<\sigma<\sigma_{III}$, interrupted at strain of ε=0.024. The white contrast in the micrographs represents dislocations. In Figure 7(a), dislocations form in column along the grain boundary passing from top to bottom in the center of the photograph, but dislocation contrast disappeared apart from the boundary. On the other hand, in Figure 7(b), dislocations are observed all over the inside of grains.

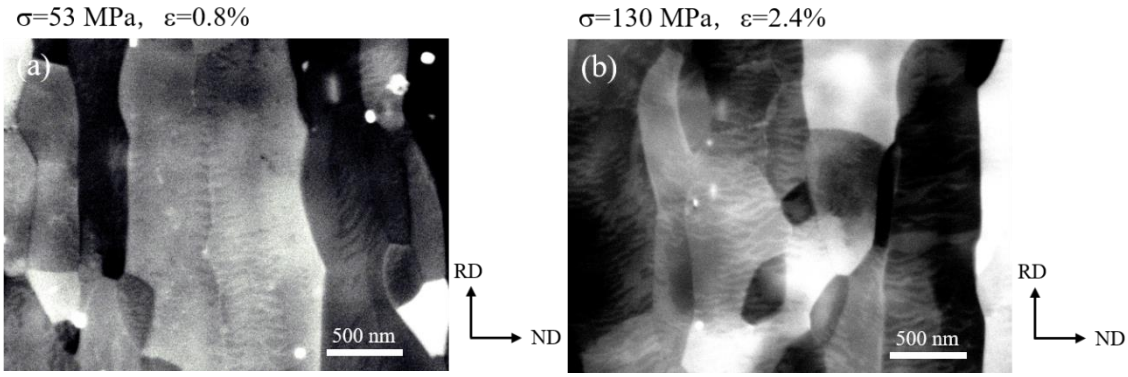

Figure 7. SEM/ECCI images obtained after the creep tests under (a) 53 MPa and (b)130 MPa for UFG aluminum of d=0.39 μm

DISCUSSION

Micro-yielding and Dislocation-Multiplication Stresses

UFG aluminum had micro-yielding stress of the same value with σ_I, below which creep does not reach steady state. It means σ_I=45 MPa corresponds to the stress which dislocation start gliding; below which negligible dislocation movement occurs resulting in very low creep deformation with a rapid decrease in strain rate at the beginning of creep.

Since rapid increase in instantaneous plastic strain above σ_{II} in Figure 6 and the observation of a certain amount of dislocation all over the inside of grains in the deformed sample in Figure 7(b), σ_{II} is considered as the stress above which the dislocation starts multiplication σ_{multi}. The multiplication of dislocations in UFG aluminum was first reported by Adachi (2015). They measured the dislocation density during tensile deformation in-situ using X-ray diffraction in SPRING-8. They found that CG aluminum start increasing the dislocation density from the very beginning of the deformation at around 0 MPa, while FG and UFG aluminum shows increase in dislocation density above respective certain stresses reffred to σ_{multi}. Our observations have coincidence with them.

In the region $\sigma_{my}<\sigma<\sigma_{multi}$, where dislocation can glide without aggressive multiplication, in addition to a small amount of the instantaneous plastic strain, dislocation density might low. Actually, Figure 7(a) shows dislocations only exist near grain boundary but scarce in the inner area of a grain. On the other hand, in the region $\sigma_{multi}<\sigma<\sigma_{0.2}$, the instantaneous plastic strain increases with increase in stress rapidly, and dislocation disperses inside of a grain as shown in Figure 7(b).

Creep Mechanism

Figure 4 shows that in the region $\sigma_I<\sigma<\sigma_{II}$ steady state creep with n=2.5, and in $\sigma_{II}<\sigma<\sigma_{III}$ steady state creep with n =7.2 occurred, respectively. Because the obtained n-value of 2.5 is close to that of 3 for low temperature creep of HCP metals (Matsunaga, 2014), the dominant creep mechanism in the region $\sigma_I<\sigma<\sigma_{II}$ might be slip-induced grain boundary sliding. That is, grain boundary sliding is observed and is thought to accommodate piled-up dislocations at grain boundaries through absorbing them. On the other hand, in the region $\sigma_{II}<\sigma<\sigma_{III}$, creep is considered to be governed by intra-grain dislocation activities because of dense dislocations inside of grains (Figure 7b). Since the obtained n-value of 7.2 is close to that of 7.0 for dislocation-core-diffusion-controlled dislocation creep at intermediate temperature above 400 K in conventional CG aluminum (Frost, 1982), the mechanism in this region inferred to dislocation-core-diffusion-controlled dislocation creep.

Matsunaga (2012) reported that UFG aluminum shows apparent activation energy of 80 kJ/mol and n-value of 6 at temperatures above 280 K, while those of 30 kJ/mol and 4 below 280 K. Their claiming higher temperature region corresponds to the region $\sigma_{II}<\sigma<\sigma_{III}$, whose creep mechanism inferred to dislocation-core-diffusion-controlled dislocation creep. On the other hand, their claiming lower temperature region corresponds to the region $\sigma_I<\sigma<\sigma_{II}$, whose creep mechanism inferred to slip-induced grain boundary sliding.

We can conclude that low temperature creep mechanisms depend on crystallographic structure but also on the temperature ranges and to the stress levels. The boundary stresses are related as σ_I: micro-yielding stress σ_{my}, σ_{II} dislocation multiplication stress σ_{multi}, and σ_{III} the 0.2% proof stress.

CONCLUSIONS

This study investigated the low-temperature creep mechanisms in ultra-fine grained aluminum made by accumulative roll bonding. The existence of steady state creep was clearly confirmed by the creep curves in the $\dot{\varepsilon}$–ε plot. The low-temperature creep behaviors in ultra-fine grained aluminum with grain size of 0.39 μm were divided into four regions by three certain stress values, σ_{my}, σ_{multi} and σ_y. σ_{my} is the stress for starting dislocation movement, σ_{multi} is the stress for starting dislocation multiplication, and $\sigma_{0.2}$ is the 0.2% proof stress. First, with stress below σ_{my}, creep deformation was negligible. Second, with stress from σ_{my} to σ_{multi}, creep deformation with n=2.5 occurred by slip-induced grain boundary sliding. Third, from σ_{multi} to σ_y, creep deformation with n=7.2 occurred by intra-granular recovery of dislocations. At last, with stress above $\sigma_{0.2}$, power-law breakdown was confirmed.

ACKNOWLEDGMENTS

This work was partially supported by The Light Metal Educational Foundation.

REFERENCES

Adachi, H., Miyajima, Y., Sato, M., & Tsuji, N. (2015). Evaluation of Dislocation Density for 1100 Aluminum with Different Grain Size during Tensile Deformation by Using In-Situ X-ray Diffraction Technique. *Mater. Trans.*, 56, 671–678.

Blum, W. (1993). High-Temperature Deformation and Creep of Crystalline Solids. In H. Mughrabi, (Ed.), *Plastic Deformation and Fracture of Materials*, (pp. 359–405), Weinheim: VCH Verlagsgesellschaft.

Blum, W. & Zeng, X.H. (2009). A simple dislocation model of deformation resistance of ultrafine-grained materials explaining Hall–Petch strengthening and enhanced strain rate sensitivity. *Acta Mater.*, 57, 1966–1974.

Frost, H.J., & Ashby, M.F. (1982). *Deformation Mechanism Maps*, Oxford: Pergamon Press.

Higane, K., Masuda, H., Tobe, H., Kitazono, K., & Sato, E. (2017). Low-temperature creep mechanism in ultrafine-grained aluminum. *J. Japan Inst. Light Metals*, 67(6), 228–233.

Kamikawa, N., Huang, X., Tsuji, N. & Hansen, N. (2009). Strengthening mechanisms in nanostructured high-purity aluminium deformed to high strain and annealed. *Acta Mater.*, 57, 4198–4208.

Kassner, M.E., Smith, K.K., & Campbell, C.S. (2015). Low-temperature creep in pure metals and alloys. *J. Mater. Sci.* 50, 6539–6551.

Matsunaga, T., Takahashi, T., Kameyama, K., & Sato, E. (2009). Relaxation mechanisms at grain boundaries for ambient-temperature creep of h.c.p. metals. *Mater. Sci. Eng.* A, 510–511, 356–358.

Matsunaga, T., Ishiwata, K., Kawai, N., & Sato, E. (2012). Grain-size dependency on creep of pure aluminum with ultra-fine grain and coarse grain at low temperatures. *J. Japan Inst. Light Metals*, 62(11), 437–441.

Matsunaga, T., & Sato, E. (2013). Creep mechanism in several grades of aluminum at low temperatures. *Mater. Trans.* 54, 2202–2208.

Neeraj, T., Hou, D.H., Daehn, G.S., & Mills, M.J. (2000). Phenomenological and microstructural analysis of room temperature creep in titanium alloys. *Acta Mater.*, 48, 1225–1238.

Saito, Y., Tsuji, N., Utsunomiya, H., Sakai, T., & Hong, R.G. (1998). Ultra-fine grained bulk aluminum produced by accumulative roll-bonding (ARB) process. *Scr. Mater.*, 39, 1221–1227.

Sato, E., Yamada, T., Tanaka, H., & Jimbo, I. (2005). Categorization of ambient temperature creep behavior of metals and alloys on their crystallographic structures, *J. Japan Inst. Light Metals*, 55(11), 604–609.